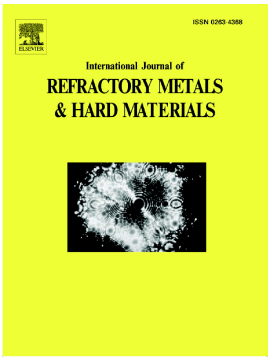

Microstructural characterization and corrosion resistance of WC-Ni-Cr-Mo composite – The effect of Mo

R.F. Santos, A.M. Ferro Rocha, A.C. Bastos, J.P. Cardoso, F. Rodrigues, C.M. Fernandes, J. Sacramento, M.G.S. Ferreira, A.M.R. Senos, C. Fonseca, M.F. Vieira, Luís F. Malheiros

PII: S0263-4368(19)30468-8

DOI: https://doi.org/10.1016/j.ijrmhm.2019.105090

Reference: RMHM 105090

To appear in: *International Journal of Refractory Metals and Hard Materials*

Received date: 13 June 2019

Revised date: 12 September 2019

Accepted date: 16 September 2019

Please cite this article as: R.F. Santos, A.M.F. Rocha, A.C. Bastos, et al., Microstructural characterization and corrosion resistance of WC-Ni-Cr-Mo composite – The effect of Mo, *International Journal of Refractory Metals and Hard Materials*(2019), https://doi.org/10.1016/j.ijrmhm.2019.105090

Microstructural characterization and corrosion resistance of WC-Ni-Cr-Mo composite – The effect of Mo

R. F. Santos[a], A. M. Ferro Rocha[b], A. C. Bastos[b], J. P. Cardoso[b], F. Rodrigues[c], C. M. Fernandes[b], J. Sacramento[c, d], M. G. S. Ferreira[b], A. M. R. Senos[b], C. Fonseca[a], M. F. Vieira[a], Luís F. Malheiros[a]

[a] INEGI – Department of Metallurgical and Materials Engineering, University of Porto, Rua Dr. Roberto Frias, 4200-465, Portugal

[b] University of Aveiro, Department of Materials and Ceramic Engineering, CICECO – Aveiro Institute of Materials, 3810-193, Aveiro, Portugal

[c] DURIT – Metalurgia Portuguesa do Tungsténio, Lda, Arruamento C – Zona Industrial, 3854-909, Albergaria-a-Velha, Portugal

[d] ESTGA – Escola Superior de Tecnologia e Gestão de Águeda, Universidade de Aveiro, Rua Comandante Pinho e Freitas, 3750-127, Águeda, Portugal

Abstract

WC-Ni-Cr-Mo are good candidates for replacing WC-Co for its better corrosion performance. This work investigated the effect of different Mo content on the mechanical properties and corrosion susceptibility of WC-Ni-Cr-Mo composites in chloride and sulphate acidic media. Chemical, microstructural, and electrochemical analysis were performed. Results show chlorides are frankly more aggressive than sulphates, but additions of up to 0.6 wt.% in Mo can enhance the active-passive transition, particularly in the presence of chlorides, and guarantee the passive state in sulphates. Also, Mo was effective in hindering WC grain growth and in increasing hardness in 5%, simultaneously reducing toughness in 4%.

Keywords

Metal matrix composites; WC; Microstructure; Acid corrosion; Passivity; Mo

1. Introduction

The demand for WC (tungsten carbide)-based composites is growing worldwide [1] namely for oil, gas, and petrochemical industries. WC-Co is the most employed system [2] since WC and

Co are considered to be a very good match regarding the mechanical properties and the manufacturing process, combining good wettability with high hardness and good toughness. However, the use of Co in these composites presents some problems. Co fails to perform desirably in corrosive environments, especially in acidic media; also, its toxicity, increasing price, and geopolitical issues involved in its primary extraction, have driven research into developing Co-poor or, preferably, Co-free binders [3].

In order to select Co substitutes, it is useful to analyse the influence of alloying elements in stainless steels. For example, Ni is added to stabilize the fcc structure of steel and to promote high toughness, Cr prompts the formation of a passive layer responsible for the high corrosion resistance which is characteristic of these alloys and Mo, when combined with Cr, is known to enhance the pitting corrosion resistance in chloride media [4-7]. Eventually, for this reason, Ni-Cr-Mo could replace the conventional use of Co in WC composites [8] for high corrosion-resistance applications.

The exact protection mechanism against pitting corrosion provided by Mo in chloride media is not clear yet but several mechanisms have been proposed to describe Mo effect in steels, such as a higher resistance of the passive film to breakdown, repassivation enhancement [9, 10], and the reduction of dissolution rate of the bare metal [11, 12]. In the presence of sulphides Mo is suggested to form a MoS protective film enhancing the corrosion resistance [13]. N. Lin *et al.* observed that adding 1 wt.% of Mo in WC-TiC-Ni composites increases significantly the corrosion resistance in chloride medium [14], which is in agreement with the findings of Qiankun Zhang *et al.*, who reported an expressive increase in corrosion resistance of the same material, where the best results were achieved at 1 and 2 wt.% of Mo for H_2SO_4 and HCl media, respectively [15]. From the microstructural point of view, Mo can beneficially inhibit grain growth of WC-based composites [16, 17].

However, although widely demonstrated for stainless steels [18-20], the impact of Mo on the corrosion resistance of WC composites is still vastly unexplored. Furthermore, issues related to the

mechanical properties of Mo-containing WC composites still exist. For example, Shengda Guo *et al*. reported that in spite of Mo capability of increasing the corrosion resistance of WC-Co hardmetals, contents over 1 wt.% become detrimental due to loss in toughness [21]. Dong *et al*. [22] concluded that the addition of 5 wt.% Mo to Ti(C, N)-based composites was able to improve their abrasion-corrosion resistance. However, contradictory results were obtained for the effects of Mo on the hardness and the toughness of these materials [23, 24].

Nonetheless, adding Mo to the binder phase reduces densification during sintering [21, 25] and increases the overall complexity and cost of the manufacturing process. In this regard, it is of great industrial interest to clarify the effects of Mo in the mechanical properties and to define the adequate Mo content that could establish the best compromise between mechanical properties and corrosion resistance. In this work, three binders based on Ni, Cr and Mo were used to investigate the impact of different Mo content on the mechanical properties and the corrosion resistance of WC-Ni-Cr-Mo alloys.

2. Experimental

2.1. Specimens preparation

The specimens were prepared from a blend of powders listed in Table 1. The powders were weighted to produce three composite grades with increasing Mo contents (0.1 to 0.6 wt.%, balanced by Ni) and mixed in ethanol in a laboratory-scale ball-milling equipment for approximately 70 hours. Afterwards, the mixture was dried out and uniaxially pressed in the form of discs (diameter 20 mm) at 15 MPa, followed by a sinter-HIP cycle up to 1440-1460ºC for 90 min (sintering stage) and under 2-3 MPa of Ar atmosphere.

Table 1 – Powders used to produce the specimens and their theoretical compositions, in wt.%

Powder	Average particle size (μm)
WC	1.2
Ni	1-2

Specimen name	Ni	Cr	Mo	WC
Mo-1	8.80	1.10	0.10	Balance
Mo-4	8.50	1.10	0.40	Balance

Cr_3C_2	1
Mo_2C	1.6

Mo-6	8.30	1.10	0.60	Balance

2.2. Chemical, mechanical and microstructural characterization

The disc specimens (20 mm diameter) were ground on a diamond (18 µm) coated disk, then polished to mirror-like surface on a cloth with a diamond (1 µm) suspension, washed in ethanol, rinsed in water and dried by air blowing at room temperature. The specimens were subsequently analysed by X-ray fluorescence, XRF (Bruker S8 Tiger), X-ray diffraction, XRD (Rigaku) with Bragg-Brentano symmetry, Cu K_α radiation and a 0.2º step, and surface observation was made by scanning electron microscopy, SEM (FEI Quanta 450). Hardness was measured through the Vickers method recommended by ISO 6507-1 (EMCO-TEST Dura Vision 20) with a load of 30 kg (5 indentations per specimen) and fracture toughness (K_{IC}) was calculated from hardness indentations by Palmqvist method used in previous works for WC-Co and WC-Ti(C, N)-Ni composites [26, 27]. The K_{IC} is defined by equation 1, where A is 0.0028, H is the hardness in $N.mm^{-2}$, P is the applied load in N and l_i is the crack length at each tip of the indentation. The grain size was measured from binary images of the microstructure of the composites on ImageJ, where more than 400 grains were measured per specimen; the average grain size was determined according to the method proposed by H. Engqvist and B. Uhrenius [28].

$$K_{IC} = A\sqrt{H}\sqrt{\frac{P}{\sum_{i=1}^{4} l_i}} \quad (1)$$

2.3. Electrochemical tests

Two acidic corrosive media were used, sodium sulphate and sodium chloride-based electrolytes, both at 0.5 M and pH between 1.5 and 2.0, adjusted by additions of H_2SO_4 and HCl, respectively. An Ag/AgCl electrode was used as the reference. The specimens' surface preparation was strictly the same for chemical, mechanical, and microstructural characterization, as previous described; this surface preparation procedure was repeated for each specimen immediately before immersion in the electrolyte solutions. A 99.6% pure Ti coil was used as counter-electrode. A

routine of electrochemical tests was executed sequentially with each specimen, as listed in Table 2 using a Gamry 1000E potentiostat. The routines were repeated three times for each specimen and a fresh portion of electrolyte was used in each routine, starting approximately one minute after specimen immersion; the exposed surface area was 0.50 cm^2. All tests were conducted at room temperature.

Table 2 – Electrochemical testing routine applied to each specimen

Routine	Parameters
Specimen cathodic cleaning	−0.5 V *vs.* reference for 300 s
Open Circuit Potential (OCP) measuring	8h *vs.* reference
Electrochemical Impedance Spectroscopy (EIS)	100,000 to 0.01 Hz (±10 mV peak *vs.* E_{oc})
Conditioning	−0.6 V *vs.* REF for 300 s
Potentiostatic polarization	−0.6 to 1.0 V (at 1 $mV.s^{-1}$)

3. Results and Discussion

3.1. Chemical and microstructural analyses

Microstructural features, such as WC particle size, distribution, and the amount of binder, are known to affect the properties and overall performance of WC-based composites [29, 30]. The WC particles are embedded in a metallic binder of Ni, Cr, and Mo, where the volumetric amount of binder was estimated by measuring its area percentage on SEM micrographs converted to binary images (Figure 1). For these measurements, a total area of about 557 μm^2 was analysed for each specimen, and values between 19.1 and 19.8% were calculated. The chemical compositions, determined by XRF in the sintered specimens, reveal a good match with powders' nominal compositions (Table 3), although Fe and Co were also found after sintering. Since the specimens were manufactured in equipment and machinery also used to produce WC-Co/Fe-based composites, Fe and Co are likely to have been introduced in the process as contamination. No phases other than WC (ICDD 00-061-0244) and Ni (ICDD 00-001-1258) with dissolved Cr and Mo were detected by XRD (Figure 2).

From the grain size distribution in Figure 3 it can be observed that the addition of 0.6 wt.% Mo can hinder WC grain growth, i.e. the number of grains ≤ 0.8 μm substantially increased. For smaller additions of Mo there is no statistically significant effect on the grain size distribution, as the small increase on the average grain size from 0.1 to 0.4 wt.% Mo is within the standard deviation. From Figure 4 it is apparent that the additions of Mo from 0.1 to 0.6 wt.% resulted in a slight decrease in fracture toughness, less than 4%, and a slight increase in hardness around 5% that can be explained by a smaller WC grain size and by the solid solution strengthening effect promoted by the Mo [31].

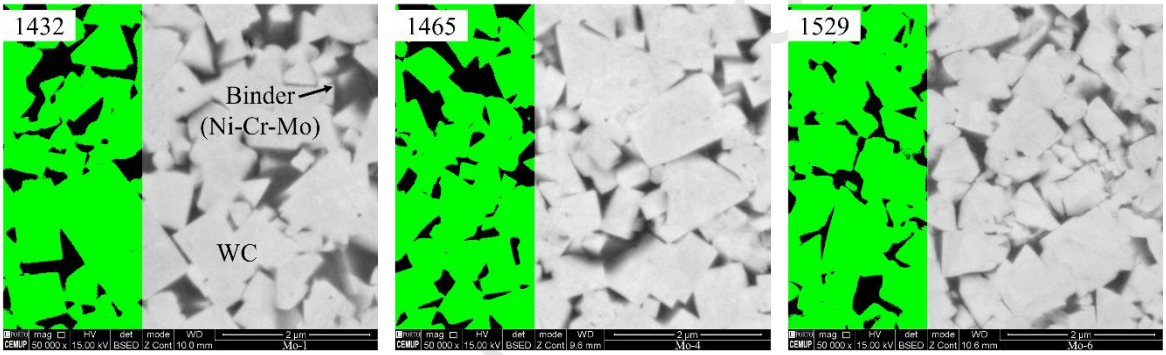

(a) (b) (c)

Figure 1 – SEM microstructures of WC-Ni-Cr-Mo, their respective binary images highlighting WC (green) and binder (black) and Vickers hardness for 0.1 (a) 0.4 (b) and 0.6 wt.% Mo (c) specimens.

Table 3 – Chemical composition measured by XRF (wt.%) and elemental content relative to binder phase only

	Overall wt. % composition						Wt. % relative to the binder phase					Binder area (%)
	Ni	Cr	Mo	Fe	Co	WC	Ni	Cr	Mo	Fe	Co	
Mo-1	9.24	0.92	0.09	0.15	0.17	Balance	87.4	08.7	0.9	1.4	1.6	19.1
Mo-4	8.66	1.11	0.43	0.28	0.05	Balance	82.2	10.4	4.1	2.7	0.5	19.8
Mo-6	9.29	1.14	0.63	0.39	0.07	Balance	80.6	09.9	5.5	3.4	0.6	19.5

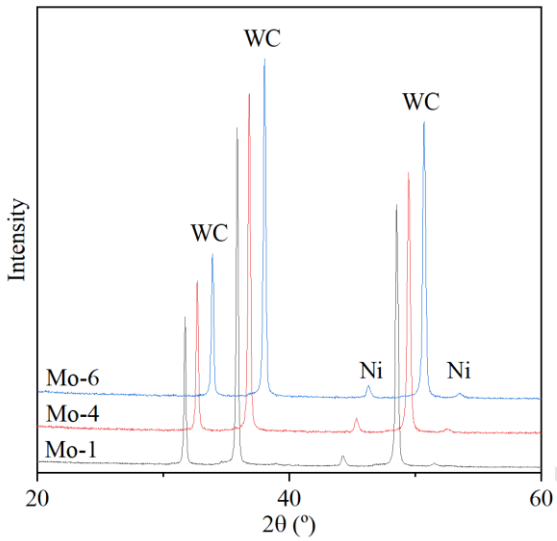

Figure 2 – X-ray diffractograms of composites revealing WC and Ni fcc phases.

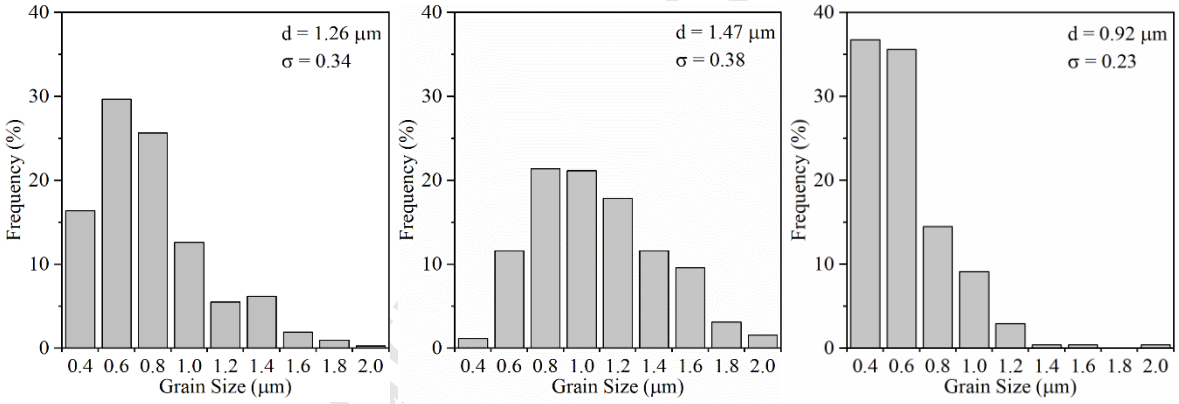

(a) (b) (c)

Figure 3 – Grain size distributions for Mo-1 (a), Mo-4 (b) and Mo-6 (c).

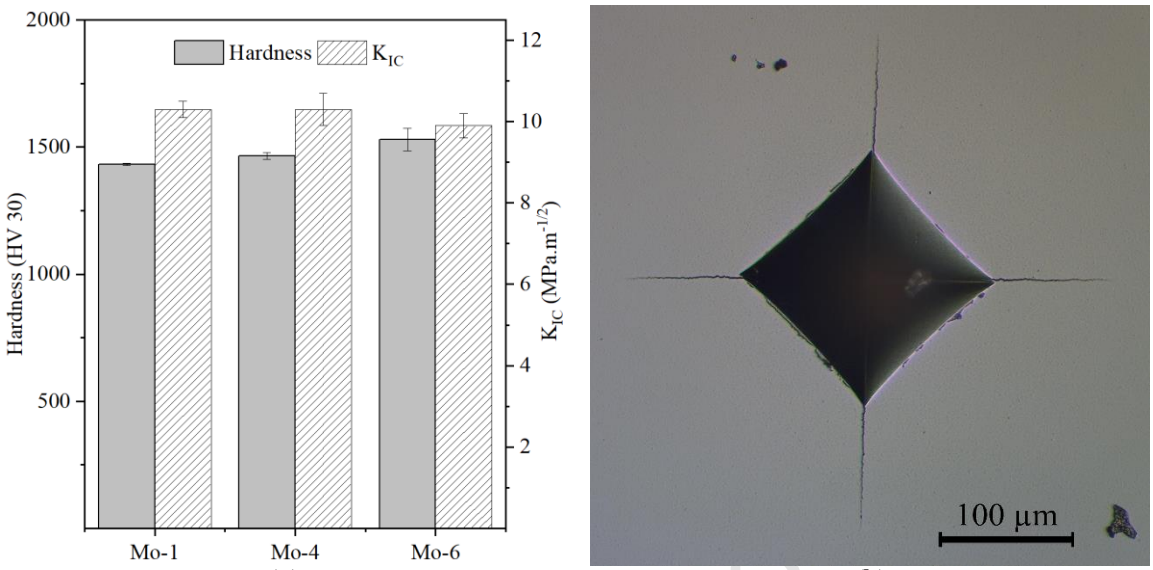

(a) (b)

Figure 4 – Mechanical properties measured for WC-Ni-Cr-Mo composites (a) and Vickers indentation mark with cracks utilized to determine toughness (a).

3.2. Open circuit measurements

Cathodic cleaning at −0.5 V during 5 minutes preceded the open circuit potential (E_{oc}) measurements that followed for 8 hours. As it can be seen from Figure 5 and Table 4, the E_{oc} values measured in the chloride medium are more cathodic than E_{oc} values obtained in the sulphate solution, around 0.15 V more negative. Within the first 4 hours, E_{oc} reaches a plateau, displaying a slight variation onwards, from −0.07 to −0.1 V and from 0.25 to 0.27 V, in the chloride and the sulphate media, respectively, which seem to be independent of the Mo content. The evolution of E_{oc} in the sulphate medium is compatible with the formation of an oxide film on the surface of the specimens that grows thicker or more insulating as the potential becomes more anodic; faster E_{oc} increase means faster oxidation kinetics, which ranks in the order Mo-6 > Mo-1 > Mo-4. The experimental data supports very consistently this ranking, however, we did not find a satisfactory explanation for such singular behaviour, which is not in line with the evolution of the Mo content of the alloys. In the chloride solution, all the three specimens exhibit a similar E_{oc} evolution; a relatively small potential increase between the beginning and the end of the measurements suggests that no significant film thickening occurs or a less protective film, e.g. a hydrated one, is formed

instead [32]. The kinetics of oxidation on the exposed surfaces, forming protective/passive films, is of special relevance when considering applications involving tribocorrosion. Faster reactions mean quicker protective film regeneration, which is essential for good performance when abrasion-corrosion is present.

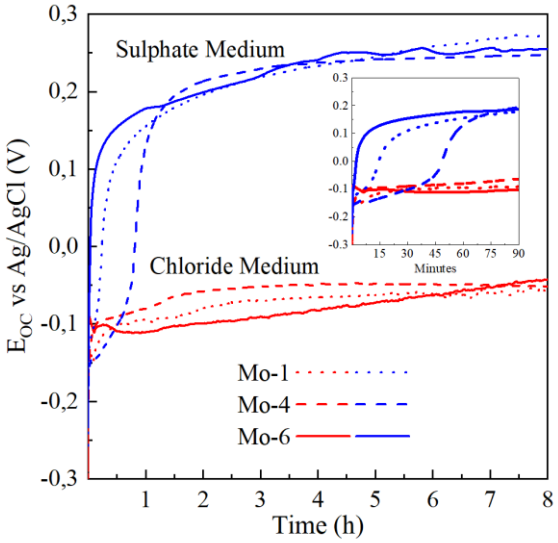

Figure 5 – Open circuit potential measurements for 8 hours of immersion.

Table 4 – Open circuit potentials after 8 hours of immersion

	E_{oc} (V)	
	Chlorides	Sulphates
Mo-1	−0.107± 0.007	0.271± 0.004
Mo-4	−0.102± 0.004	0.253± 0.003
Mo-6	−0.076± 0.031	0.250± 0.021

3.3. Potentiostatic polarization

The voltammograms of the WC-composites are plotted in Figure 6. In chloride medium, the three grades display a current peak at potentials close to 0.0 V (Figure 6a). However, in the case of Mo-6, unlike in Mo-1 and Mo-4, a steeper current decrease of about one order of magnitude can be identified. Mo-6 also displays lower currents in the anodic potential range. However, such current decrease around 0.0 V should also be partially ascribed to the presence of Cr, through the formation of chromium oxide. Indeed, it has been shown that WC-Co-Cr exhibits enhanced active-passive

transition and corrosion resistance in acidic media containing chlorides, whereas WC-Co [33] and WC-Ni [15] do not passivate in the same conditions. This latter investigation showed that although WC-TiC-Ni-Mo grades without Cr presented a notable decrease in current density, it was observed in the range of 0.6 to 1.0 V, more than 0.5 V higher than that observed in this work for WC-Ni-Cr-Mo, suggesting that the Cr-Mo combination is also responsible for shifting the active-passive transition to lower potential values.

For the alloys used in this work, Cr represents 10 wt.% of the binder (Table 3) which is slightly below the lower limit for corrosion resistance required in stainless steels, yet its effect in promoting a passivated state is still clearly visible here. Nevertheless, all specimens used for this work possess a similar Cr content, which means that the more enhanced active-passive transition of Mo-6 in chloride solution should be attributed to its higher Mo content. This effect of Mo in promoting passivation is in agreement with the findings of the aforementioned investigation on WC-TiC-Ni-Mo. Although exhibiting a significant decrease in current density at roughly 0.1 V, the lowest current densities measured for specimens Mo-1 and Mo-4 are approximately 100 and 150 $\mu A.cm^{-2}$, respectively, measured for a narrow potential range, which is considered to be incompatible with a passivated state (Figure 6a). Mo-6 presents the best performance, displaying a current density of 14 $\mu A.cm^{-2}$.

In sulphate medium (Figure 6b), anodic passivation is clearly granted for the three alloy compositions. The active-passive peak (at −0.05 V) is less pronounced than the one measured in chloride environment, meaning that the passive state is easier to achieve in the absence of Cl^- ions, and that decreases with the Mo content, showing the beneficial effects of Mo in the passivation process. Outstandingly, the Mo-6 alloy does not show an active-passive transition behaviour when it enters the anodic branch of the polarization curve, meaning that a higher Mo content leads to a quicker passivation. This is in good agreement with the OCP curves in Figure 5, where Mo-6 displays faster oxidation kinetics. It is possible that the strong negative potential applied before the

polarization tests, −0.6 V, dissolved, in some extent at least, the passive films formed on the surface of Mo-1 and Mo-4 after the 8-hour immersion; this would explain the presence of active-passive transition peaks associated with a repassivation process on such alloys. The film formed on the surface of Mo-6, however, may have suffered lesser dissolution and/or was capable of repassivating quicker, before entering the anodic branch, probably due to its higher Mo content. It is interesting to note that in sulphate medium the current peak of Mo-1 has a lower magnitude than that of Mo-4, around −0.1 V (Figure 6b). This lower anodic current peak of Mo-1 compared to Mo-4 can be explained if one considers that Mo-1 was faster to repassivate. Such behaviour is coherent with a quicker passivation displayed by Mo-1 relatively to Mo-4 as revealed by the E_{oc} measurements shown in Figure 1 and already discussed in section 3.2. The lowest current densities in the passive region are roughly 2.6 $\mu A.cm^{-2}$ in Mo-4 and Mo-6, and 3.4 $\mu A.cm^{-2}$ in Mo-1, in a potential range between 0.2 and 0.4 V.

Table 5 presents the corrosion potentials (E_{corr}) and the corrosion currents (i_{corr}) determined from the Tafel region of the anodic branch in voltammetry curves. Mo-6 is the best performing alloy, displaying the most noble corrosion potential and the lowest corrosion current values in each media. Mo-4 shows the highest i_{corr}, which is more notable among the specimens exposed to sulphate medium, and the least noble E_{corr}. These findings point out that intermediate Mo content seems to be slowing down passivation kinetics and increasing the corrosion suscetibility. The overall higher i_{corr} found for alloys in chloride environment highlights its stronger aggressiveness when compared with sulphate medium.

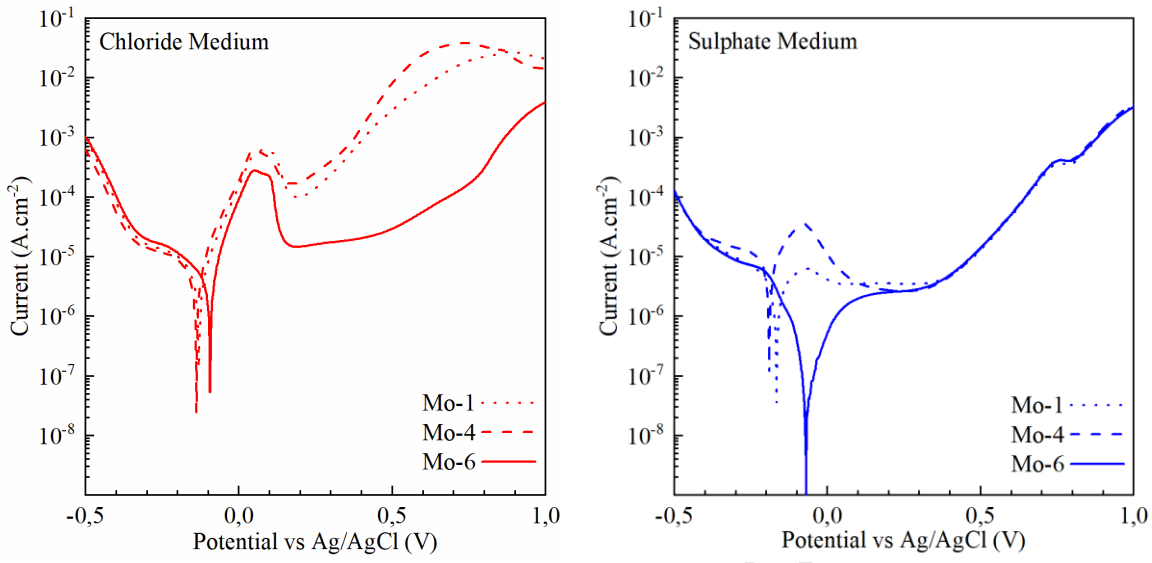

Figure 6 – Polarization curves in chloride (a) and sulphate media (b).

Table 5 – Corrosion potentials and currents

	Chlorides		Sulphates	
	E_{corr} (V)	i_{corr} (μA.cm^{-2})	E_{corr} (V)	i_{corr} (μA.cm^{-2})
Mo-1	−0.120 ±0.006	17 ±1	−0.167 ±0.002	03.8 ±0.8
Mo-4	−0.130 ±0.007	23.17 ±2.98	−0.186 ±0.002	15 ±3
Mo-6	−0.075± 0.036	16.84± 4.53	−0.063± 0.056	00.2± 0.2

3.4. Electrochemical impedance spectroscopy

The Bode spectra for the WC-based composites are reported in Figure 7. Given the simple shape of the curves, where only on time constant seems to be present, the electrical circuit of Figure 7 was chosen to describe the WC-based composites/solution interface, where R_{sol} stands for the solution resistance and R_p stands for the polarization resistance (in cases where there is no protective film) or for film resistance (in cases where there is a passivating film). The capacitive element in parallel with R_p was replaced by a constant phase element (CPE) to take into account for the roughness and/or other surface inhomogeneities or relaxation processes occurring at the interface [17]. The impedance Z of a CPE can be defined by equation 2:

$$Z_{CPE} = \frac{1}{Y_0(j\omega)^{\alpha}} \quad (2)$$

where Y_0 and α are the CPE parameters and ω is the angular frequency ($\omega = 2\pi f$). The fittings of the EIS data according to the chosen equivalent circuit are plotted also in Figure 7, overlaid on the corresponding experimental data points. The ability of the proposed circuit to describe the experimental data in both media is excellent (Figure 7), and the resulting fitting parameters are reported in Table 6. The capacitances (C) of the specimen-solution interface were calculated from the circuit parameters according to equation 3 [34]:

$$C = \sqrt[\alpha]{\frac{Y_0 R_p}{{R_p}^{\alpha}}} \quad (3)$$

The values of R_p differ from the chloride to the sulphate media by about three orders of magnitude, a consequence of the formation of thicker (or more insulating) films in the sulphate environment, as it was already concluded from the evolution of the E_{oc} values (Figure 5 and Table 4) and from the voltammograms of Figure 6, namely the active-passive peak current and passivation currents. Therefore, from the high R_p values in the sulphate medium (in the MΩ range), passivation takes place, whereas in the chloride solution if a film eventually exists it is not effective in protecting the material against corrosion, as the system display R_p values in the kΩ range. The higher aggressiveness of chloride medium for WC-Co alloys was already reported by other authors [35].

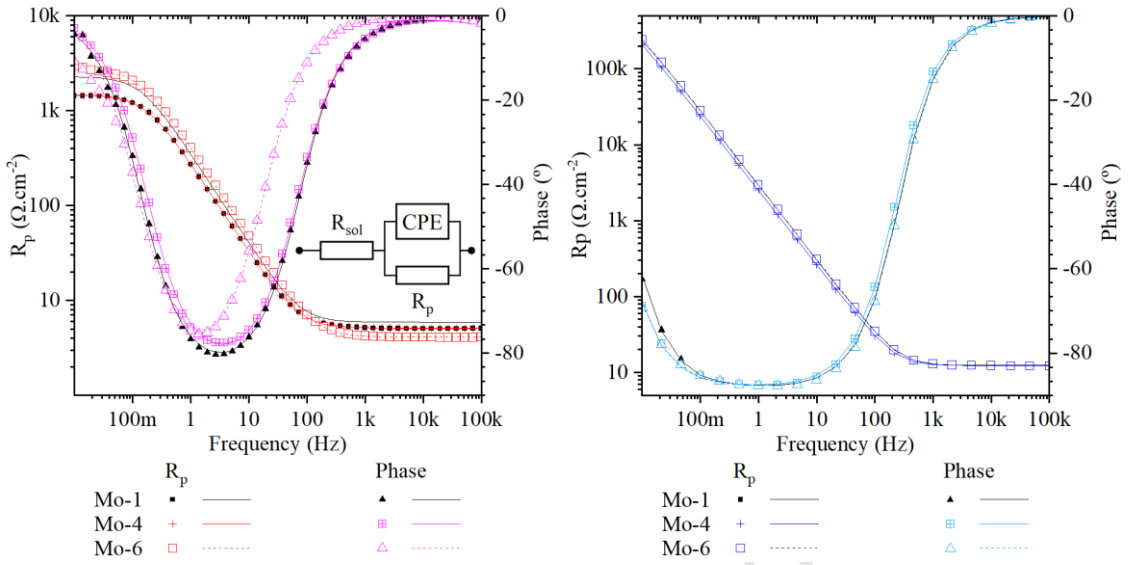

Figure 7 – Bode and phase diagrams of experimental data points and fitting curves for chlorides (a) and sulphates (b).

The highest R_p values were found in both media for the Mo-6, demonstrating that 0.6 wt.% Mo is effective in protecting against corrosion of WC-composites in acidic media. The α values of the CPE are close to 1, which is associated with an essentially capacitive behaviour of the CPE. The capacitances of the specimen-solution interface in chloride medium are all higher than those in sulphate solution, where Mo-6 displays the lower capacitance in each media (Table 6). These findings are compatible with the formation of a more protective layer (higher Cr or Mo content, or with fewer defects), or a thicker film in Mo-6, particularly in sulphate medium, if one assumes a constant relative electric permittivity. The collective results suggest that 0.6 wt.% Mo can effectively enhance corrosion resistance, but intermediate Mo content may exert a detrimental effect on the corrosion susceptibility of WC-Ni-Cr-Mo alloys, although the reasons and mechanisms behind such negative impact could not be provided by this study. Evidently, only a detailed specimen surface analysis after immersion could confirm the presence of any interfacial films, their structural and chemical characteristics, and could provide insight about such deleterious effect.

Table 6 – Polarization and electrolyte resistances, CPE, and capacitance values determined by EIS

	Chloride Medium				
	R_p	R_{sol}	Y_0	α	C
	$\Omega.cm^2$	$\Omega.cm^2$	$\Omega^{-1}.s^{\alpha}.cm^{-2}$		F
Mo-1	$1.85x10^{3}$ $\pm 2.9x10^{2}$	4.54 ±1.35	$5.27x10^{-4}$ $\pm 2.3x10^{-5}$	$9.43x10^{-1}$ $\pm 4x10^{-3}$	$5.25x10^{-4}$ $\pm 2.3x10^{-5}$
Mo-4	$1.45x10^{3}$ $\pm 1x10^{1}$	3.87 ±1.22	$6.71x10^{-4}$ $\pm 4.0x10^{-5}$	$9.35x10^{-1}$ $\pm 5x10^{-3}$	$6.70x10^{-4}$ $\pm 4.2x10^{-5}$
Mo-6	$3.25x10^{3}$ $\pm 1.15x10^{3}$	11.6 ±5.0	$4.88x10^{-4}$ $\pm 9.4x10^{-5}$	$9.47x10^{-1}$ $\pm 4x10^{-3}$	$4.98x10^{-4}$ $\pm 9.4x10^{-5}$
	Sulphate Medium				
Mo-1	$1.06x10^{6}$ $\pm 5.39x10^{4}$	24.53 ±0.12	$2.86x10^{-5}$ $\pm 4x10^{-7}$	$9.80x10^{-1}$ $\pm 3x10^{-4}$	$3.06x10^{-5}$ $\pm 2x10^{-7}$
Mo-4	$1.27x10^{6}$ $\pm 5.79x10^{4}$	24.58 ±0.18	$3.26x10^{-5}$ $\pm 8x10^{-7}$	$9.78x10^{-1}$ $\pm 4x10^{-4}$	$3.55x10^{-5}$ $\pm 8x10^{-7}$
Mo-6	$1.41x10^{6}$ $\pm 1.47x10^{5}$	24.89 ±0.45	$2.79x10^{-5}$ $\pm 3x10^{-7}$	$9.80x10^{-1}$ $\pm 1x10^{-3}$	$3.00x10^{-5}$ $\pm 4x10^{-7}$

5. Conclusions

Mechanical properties and corrosion susceptibility of three WC-Ni-Cr-Mo (with increasing Mo content) was tested in acidic chloride and sulphate media. The chloride environment was frankly more aggressive than its sulphate counterpart, although Mo presented visible benefits in contents of 0.6 wt.% for improved corrosion resistance in WC-Ni-Cr-based composites, effectively enhancing the anodic active-passive transition in chloride medium and ensuring the passivated state in sulphate solution. Mo content of 0.6 wt.% Mo was also effective in hindering WC grain growth and increasing hardness by 5%, with a slight decrease in toughness of 4%, making Ni-Cr-Mo a very interesting candidate to replace Co as a binder for WC-based composites; intermediate additions of 0.4 wt.% Mo appear to be detrimental, contributing for a small increase in corrosion susceptibility.

Acknowledgments

This research work was financed by Portugal 2020 through European Regional Development Fund (FEDER) in the frame of Operational Competitiveness and Internationalization Programme (POCI) and the scope of the project HARDCorr (POCI-01-0247-FEDER-003382).

References

[1] S. Norgren, J. García, A Blomqvist, L. Yin, **Trends in the P/M hard metal industry**, Int. J. Refract. Met. H. 48 (2015) 31-45. https://doi.org/10.1016/j.ijrmhm.2014.07.007.

[2] Samuel A. Humphry-Baker, Ke Peng, William E. Lee, **Oxidation resistant tungsten carbide hardmetals**, Int. J. Refract. Met. H. 66 (2015) 135-143. https://doi.org/10.1016/j.ijrmhm.2017.03.009.

[3] Laura Leyssens, Bart Vinck, Catherine Van Der Straeten, Floris Wuyts, Leen Maes, **Cobalt toxicity in humans—A review of the potential sources and systemic health effects**, Toxicology 387 (2017) 43-56. https://doi.org/10.1016/j.tox.2017.05.015.

[4] Li-cong AN, Jing CAO, Lin-cai WU, Hong-huan MAO, Yi-tao YANG, **Effects of Mo and Mn on Pitting Behavior of Duplex Stainless Steel**, J. Iron. Steel Res. Int. 23 (2016) 1333-1341. https://doi.org/10.1016/S1006-706X(16)30196-0.

[5] A. Pardo, M. C. Merino, A. E. Coy, F. Viejo, R. Arrabal, E. Matykina, **Pitting corrosion behaviour of austenitic stainless steels – combining effects of Mn and Mo additions**, Corros. Sci. 50 (2008) 1796-1806. https://doi.org/10.1016/j.corsci.2008.04.005.

[6] Katsuhisa Sugimoto and Yoshinobu Sawada, **The role of alloyed molybdenum in austenitic stainless steels in the inhibition of pitting in neutral halide solutions**, Corrosion 32 (1976) 347-352. https://doi.org/10.5006/0010-9312-32.9.347.

[7] R. Qvarfort, **Some observations regarding the influence of molybdenum on the pitting corrosion resistance of stainless steels**, Corros. Sci. 40 (1998) 215-223. https://doi.org/10.1016/S0010-938X(97)00118-2.

[8] A. M. Ferro Rocha, A. C. Bastos, J. P. Cardoso, F. Rodrigues, C. M. Fernandes, E. Soares, J. Sacramento, A. M. R. Senos, M. G. S. Ferreira, **Corrosion behaviour of WC hardmetals with nickel-based binders**, Corros. Sci. 147 (2019) 384-393. https://doi.org/10.1016/j.corsci.2018.11.015.

[9] C. R. Clayton and Y. C. Lu, **A Bipolar Model of the Passivity of Stainless Steel: The Role of Mo Addition**, J. Electrochem. Soc. 133 (1986) 2465-2473. https://doi.org/10.1002/chin.198714026.

[10] Y. C. Lu, C. R. Clayton, A. R. Brooks, **A bipolar model of the passivity of stainless steels—II. The influence of aqueous molybdate**, Corros. Sci. 29 (1989) 863-880. https://doi.org/10.1016/0010-938X(89)90058-9.

[11] M. Kaneko and H. S. Isaacs, **Effects of molybdenum on the pitting of ferritic- and austenitic-stainless steels in bromide and chloride solutions**, Corros. Sci. 44 (2002) 1825-1834. https://doi.org/10.1016/S0010-938X(02)00003-3.

[12] N. Boucherit, A. Hugot-Le Goff, S. Joiret, **Influence of Ni, Mo, and Cr on Pitting Corrosion of Steels Studied by Raman Spectroscopy**, Corrosion 48 (1992) 569-579. https://doi.org/10.5006/1.3315974.

[13] Akiko Tomio, Masayuki Sagara, Takashi Doi, Hisashi Amaya, Nobuo Otsuka, Takeo Kudo, **Role of alloyed molybdenum on corrosion resistance of austenitic Ni-Cr-Mo-Fe alloys in H2S-Cl^- environments**, Corros. Sci. 98 (2015) 391-398. https://doi.org/10.1016/j.corsci.2015.05.053.

[14] N. Lin, C. H. Wu, Y. H. He, D. F. Zhang, **Effect of Mo and Co additions on the microstructure and properties of WC-TiC-Ni cemented carbides**, Int. J. Refract. Met. H. 30 (2012) 107-113. https://doi.org/10.1016/j.ijrmhm.2011.07.011.

[15] Qiankun Zhang, Nan Lin, Yuehui He, **Effects of Mo additions on the corrosion behavior of WC-TiC-Ni hardmetals in acidic solutions**, Int. J. Refract. Met. H. 38 (2013) 15-25. https://doi.org/10.1016/j.ijrmhm.2012.12.003.

[16] Lukas Lauter, Roman Hochenauer, Chirstoph Buchegger, Marcel Bohn, Walter Lengauer, **Solid-state solubilities of grain-growth inhibitors in WC-Co and WC-MC-Co hardmetals**, J. Alloy Compd. 675 (2016) 407-415. https://doi.org/10.1016/j.jallcom.2016.03.117.

[17] S. G. Huang, J. Vleugels, H. Mohrbacher, M Woydt, **Microstructure and tribological performance of NbC-Ni cermets modified by VC and Mo_2C**, Int. J. Refract. Met. H. 66 (2017) 188-197. https://doi.org/10.1016/j.ijrmhm.2017.03.012.

[18] A. Pardo, M. C. Merino, A. E. Coy, F. Viejo, R. Arrabal, E. Matykina, **Effect of Mo and Mn additions on the corrosion behaviour of AISI 304 and 316 stainless steels in H_2SO_4**, Corros. Sci. 50 (2008) 780-794. https://doi.org/10.1016/j.corsci.2007.11.004.

[19] Jun Shu, Hongyun Bi, Xin Li, Zhou Xu, **The effect of copper and molybdenum on pitting corrosion and stress corrosion cracking behavior of ultra-pure ferritic stainless steels**, Corros. Sci. 57 (2012) 89-98. https://doi.org/10.1016/j.corsci.2011.12.030.

[20] Seok Joo Doh, Jung Ho Je, Jin Suk Kim, Kyoo Young Kim, Hee San Kim, Young Duk Lee, Jay Min Lee, Yeukuang Hwu, **Influence of Cr and Mo on the passivation of stainless steel 430 (18Cr) and 444 (18Cr–2Mo): In situ XANES study**, Nucl. Instrum. Meth. B. 199 (2003) 211-215. https://doi.org/10.1016/S0168-583X(02)01548-3.

[21] Shengda Guo, Jiangao Yang, Hao Chen, Jianhong Yi, **Effect of Mo and Y_2O_3 additions on the microstructure and properties of fine WC-Co cemented carbides fabricated by spark plasma sintering**, Int. J. Refract. Met. H. 69 (2017) 1-10. https://doi.org/10.1016/j.ijrmhm.2017.07.010.

[22] Guangbiao Dong, Ji Xiong, Mei Yang, Zhixing Guo, Weicai Wan, **Effect of Mo_2C on erosion–corrosion resistance behavior of Ti(C, N)-based cermets**, Wear 294-295 (2012) 364-369. https://doi.org/10.1016/j.wear.2012.05.013.

[23] Ehsan Ghasali, Touradj Ebadzadeh, Masoud Alizadeh, Mansour Razavi, **Mechanical and microstructural properties of WC-based cermets: A comparative study on the effect of Ni and Mo binder phases**, Ceram. Int. 44 (2018) 2283-2291. https://doi.org/10.1016/j.ceramint.2017.10.189.

[24] Zhenye Zhao, Jianwei Liu, Huaguo Tang, Xianfeng Ma, Wei Zhao, **Effect of Mo addition on the microstructure and properties of WC–Ni–Fe hard alloys**, J. Alloy Compd. 646 (2015) 155-160. https://doi.org/10.1016/j.jallcom.2015.05.277.

[25] R. M. Genga, L. A. Cornish, G. Akdogan, **Effect of Mo_2C additions on the properties of SPS manufactured WC-TiC-Ni cemented carbides**, Int. J. Refract. Met. H. 41 (2013) 12-21. https://doi.org/10.1016/j.ijrmhm.2013.01.008.

[26] W. D. Schubert, H. Neumeister, G. Kinger, B. Lux, **Hardness to toughness relationship of fine-grained WC-Co hardmetals**, Int. J. Refract. Met. H. 16 (1998) 133-142. https://doi.org/10.1016/S0263-4368(98)00028-6.

[27] Yuemei Wu, Ji Xiong, Zhixing Guo, Mei Yang, Jianzhong Chen, Sujian Xiong, Hongyuan Fan, Jianjun Luo, **Microstructure and fracture toughness of $Ti(C_{0.7}N_{0.3})$-WC-Ni cermets**, Int. J. Refract. Met. H. 29 (2011) 85-89. https://doi.org/10.1016/j.ijrmhm.2010.08.004.

[28] H. Engqvist and B. Uhrenius, **Determination of the average grain size of cemented carbides**, Int. J. Refract. Met. H. 21 (2002) 31-35. https://doi.org/10.1016/S0263-4368(03)00005-2.

[29] Hiroyuki Saito, Akira Iwabuchi, Tomoharu Shimizu, **Effects of Co content and WC grain size on wear of WC cemented carbide**, Int. J. Refract. Met. H. 261 (2006) 126-132. https://doi.org/10.1016/j.wear.2005.09.034.

[30] Li Zhang, Yi Chen, Qing-lei Wan, Ting Liu, Ji-fei Zhu, Wei Tian, **Electrochemical corrosion behaviors of straight WC–Co alloys: Exclusive variation in grain sizes and aggressive media**, Int. J. Refract. Met. H. 57 (2016) 70-77. https://doi.org/10.1016/j.ijrmhm.2016.02.009.

[31] Sean R. Agnew, Liang Dong, Jasmine I. Keene, Haydn N. G. Wadley, **Mechanical properties of large TiC-Mo-Ni cermet tiles**, Int. J. Refract. Met. H. 75 (2018) 238-247. https://doi.org/10.1016/j.ijrmhm.2018.05.005.

[32] J. M. Abd El Kader and A. M. Shams El Din, **Film thickening on nickel in aqueous solution in relation to anion type and concentration**, Br. Corros. J. 14 (1979) 40-45. https://doi.org/10.1179/000705979798276022.

[33] W. J. Tomlinson, N. J. Ayerst, **Anodic polarization and corrosion of WC-Co hardmetals containing small amounts of Cr_3C_2 and/or VC**, J. Mater. Sci. 24 (1989) 2348-2352. https://doi.org/10.1007/BF01174495.

[34] Evgenij Barsoukov and J. Ross Macdonald, **Impedance Spectroscopy: Theory, Experiment, and Applications**, 3rd ed. Hoboken: Wiley; 2018.

[35] Sutha Sutthiruangwong and Gregor Mori, **Corrosion properties of Co-based cemented carbides in acidic solutions**, Int. J. Refract. Met. H. 21 (2003) 135-145. https://doi.org/10.1016/S0263-4368(03)00027-1.

Highlights

- Microstructure of WC-Ni-Cr-Mo composite
- Mo additions up to 0.6 wt.% can improve corrosion resistance
- Intermediate Mo additions can have detrimental impact on corrosion susceptibility
- Chlorides are expressively more aggressive than sulphates to the binder phase
- Mechanical properties do not change significantly

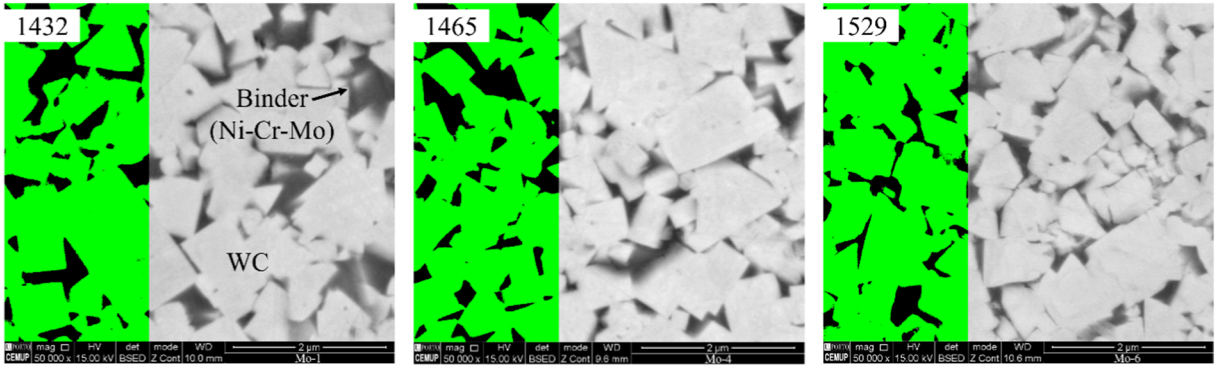

(a) (b) (c)

Figure 1

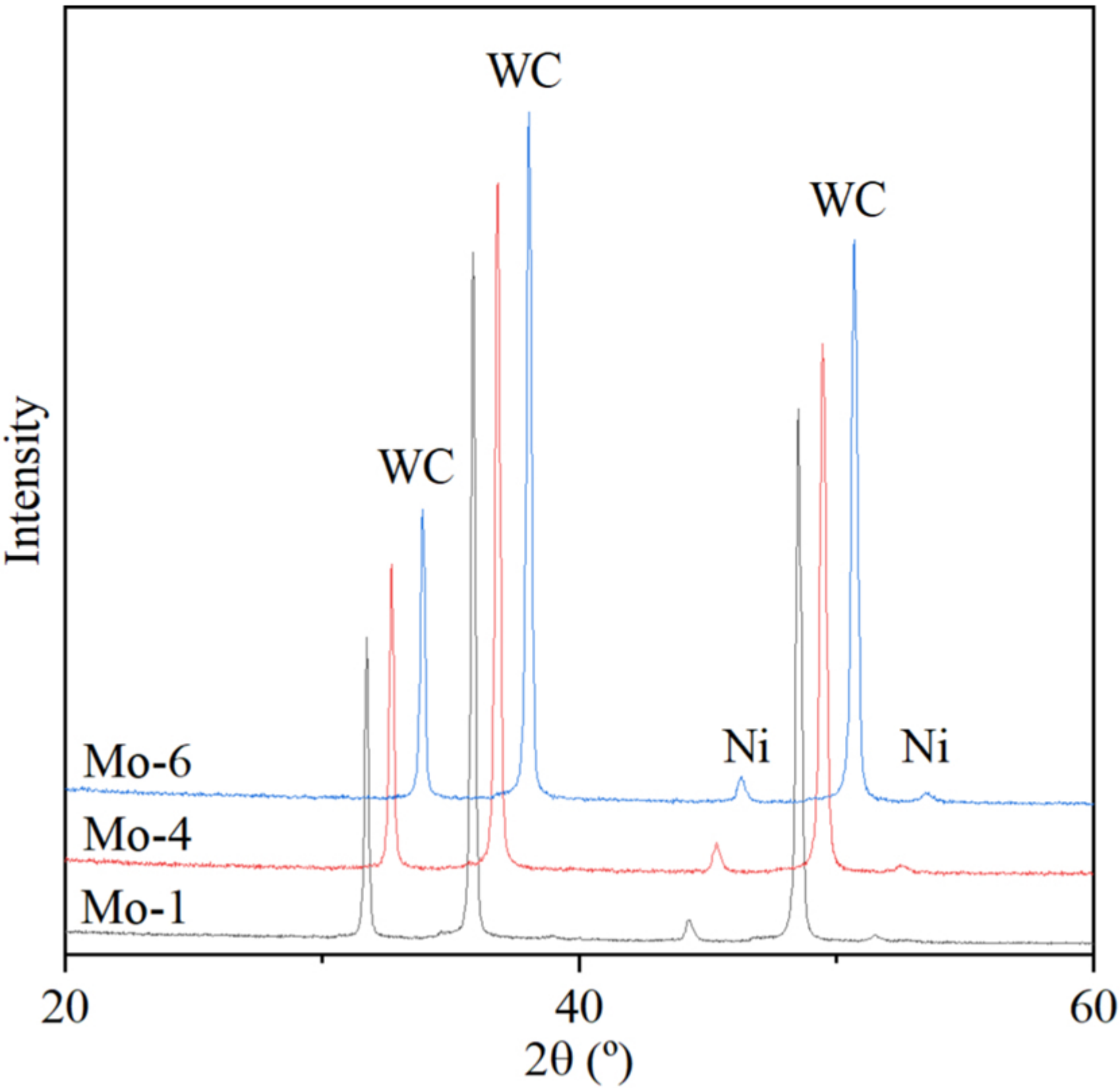

Figure 2

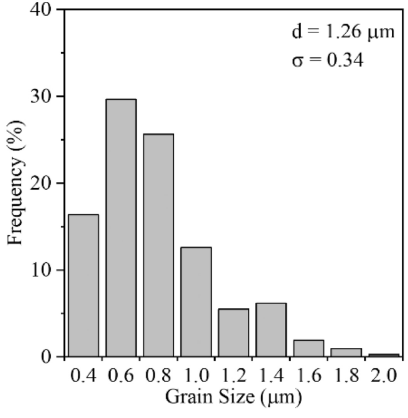
d = 1.26 μm
σ = 0.34
Frequency (%)
Grain Size (μm)
0.4 0.6 0.8 1.0 1.2 1.4 1.6 1.8 2.0
0 10 20 30 40

(a)

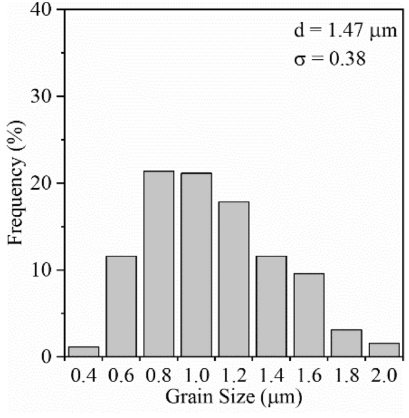
d = 1.47 μm
σ = 0.38
Frequency (%)
Grain Size (μm)
0.4 0.6 0.8 1.0 1.2 1.4 1.6 1.8 2.0
0 10 20 30 40

(b)

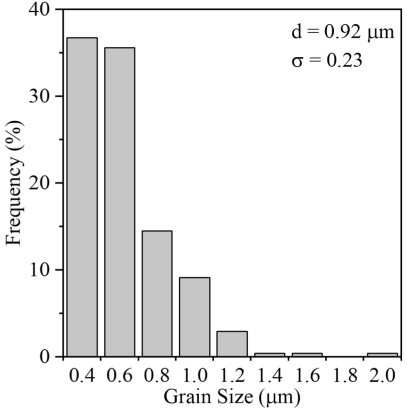
d = 0.92 μm
σ = 0.23
Frequency (%)
Grain Size (μm)
0.4 0.6 0.8 1.0 1.2 1.4 1.6 1.8 2.0
0 10 20 30 40

(c)

Figure 3

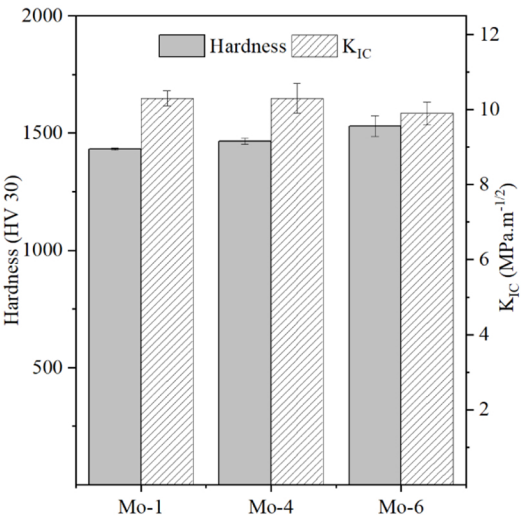
Hardness
K_{IC}
Hardness (HV 30)
K_{IC} (MPa.m$^{-1/2}$)
2000
1500
1000
500
12
10
8
6
4
2
Mo-1
Mo-4
Mo-6

(a)

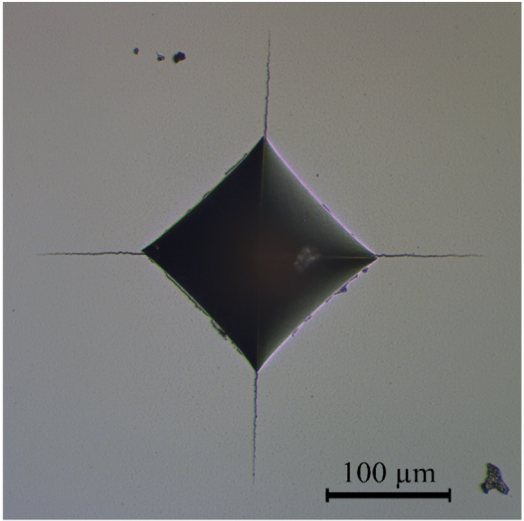
100 µm

(b)

Figure 4

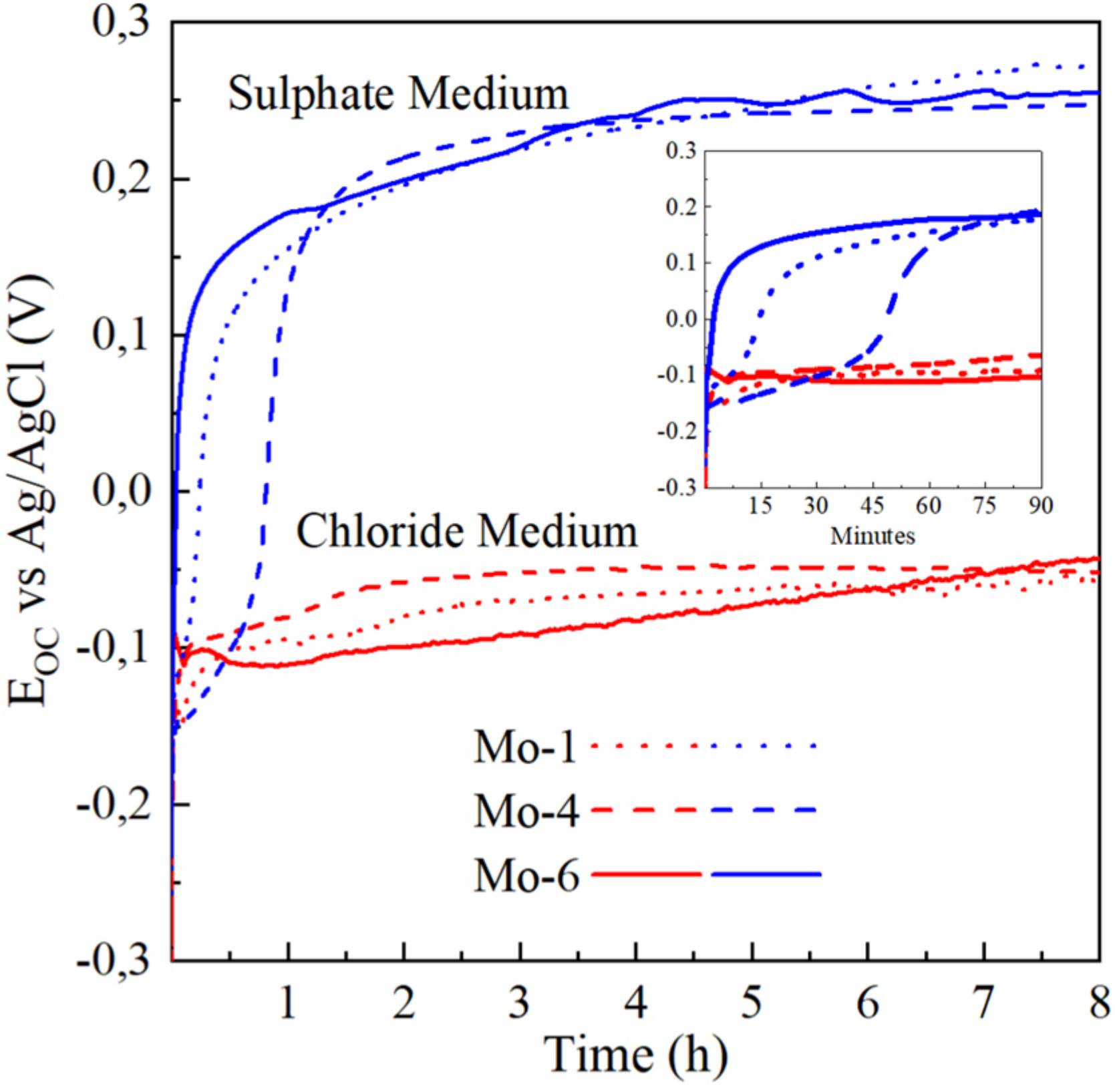
Sulphate Medium
Chloride Medium
Mo-1
Mo-4
Mo-6
E_{OC} vs Ag/AgCl (V)
Time (h)
0,3
0,2
0,1
0,0
-0,1
-0,2
-0,3
1
2
3
4
5
6
7
8
0.3
0.2
0.1
0.0
-0.1
-0.2
-0.3
15
30
45
60
75
90
Minutes

Figure 5

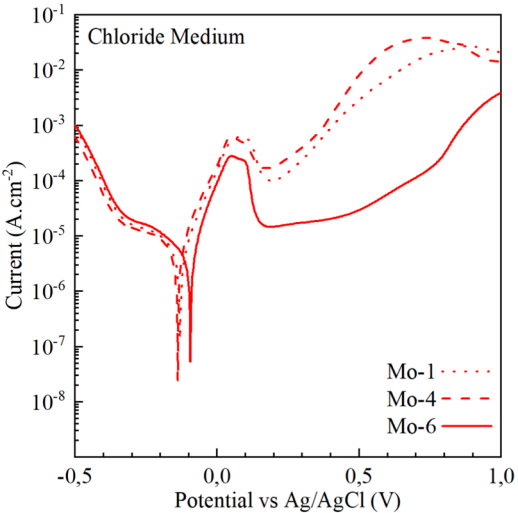
Chloride Medium
Current (A.cm-2)
Potential vs Ag/AgCl (V)
Mo-1
Mo-4
Mo-6
(a)

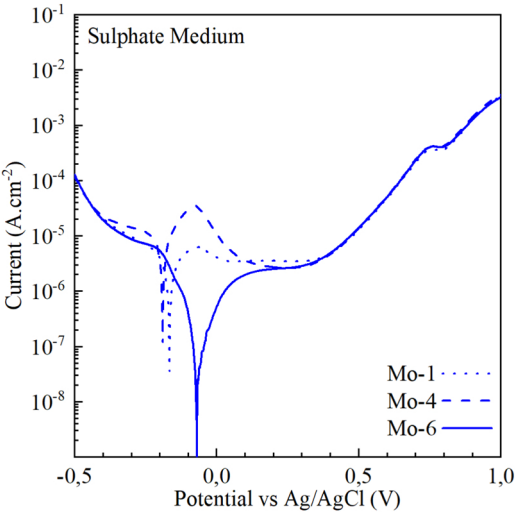
Sulphate Medium
Current (A.cm-2)
Potential vs Ag/AgCl (V)
Mo-1
Mo-4
Mo-6
(b)

Figure 6

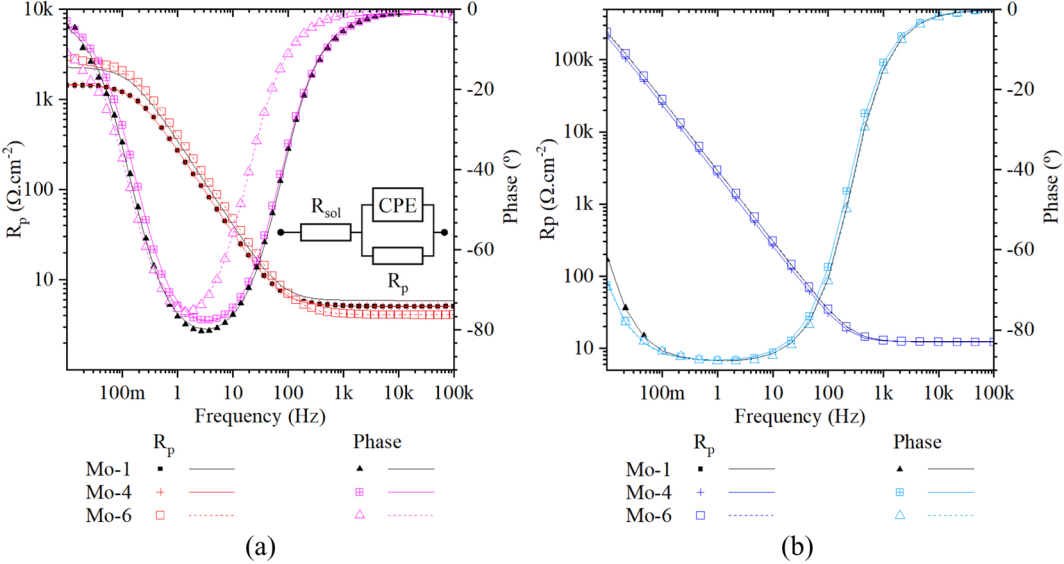
10k
1k
100
10
R_p ($\Omega.cm^{-2}$)
0
-20
-40
-60
-80
Phase (°)
R_{sol}
CPE
R_p
100m
1
10
100
1k
10k
100k
Frequency (Hz)
R_p
Phase
Mo-1
Mo-4
Mo-6
(a)
100k
10k
1k
100
10
Rp ($\Omega.cm^{-2}$)
0
-20
-40
-60
-80
Phase (°)
100m
1
10
100
1k
10k
100k
Frequency (Hz)
R_p
Phase
Mo-1
Mo-4
Mo-6
(b)

Figure 7